Lattice dynamics of cubic $NaNbO_3$: An inelastic neutron scattering study

Izumi Tomeno*
Faculty of Education and Human Studies, Akita University, Akita 010-8502, Japan

Yorihiko Tsunoda
Department of Applied Physics, School of Science and Engineering, Waseda University, Shinjuku, Tokyo 169-8555, Japan

Kunihiko Oka
Nanoelectronics Research Institute, National Institute of Advanced Industrial Science and Technology, Tsukuba, Ibaraki 305-8568, Japan

Masato Matsuura† and Masakazu Nishi
Institute for Solid State Physics, University of Tokyo, Kashiwa 277-8581, Japan

(Received 25 February 2009; revised manuscript received 7 August 2009; published 4 September 2009)

The phonon-dispersion relations for cubic $NaNbO_3$ have been determined along the [100], [110], and [111] directions using inelastic neutron scattering. A simultaneous softening of transverse acoustic (TA) phonon modes occurs at the zone-boundary $M(0.5,0.5,0)$ and $R(0.5,0.5,0.5)$ points, indicating the instabilities of in-phase and out-of-phase rotations of the oxygen octahedra about the [001] direction. These zone-boundary modes exhibit an extremely gradual softening as the temperature is lowered toward $T_{c1}=913$ K. The inelastic diffuse scattering at the $M(0.5,0.5,0)$ point polarized along the $[1\bar{1}0]$ direction remains up to 9 meV, whereas the inelastic diffuse scattering at the M point polarized along the [001] direction is suppressed. Polarization dependence shows that the inelastic diffuse scattering at the M and R points originates from the dynamical motion of oxygen octahedra. The transverse optic (TO) phonon modes along the [110] direction polarized with the [001] direction also soften around $\mathbf{q}=[0.15,0.15,0]$ and merge into the lower-energy TA phonon modes. This is basically similar to the waterfall phenomenon observed for Pb-based perovskite relaxor ferroelectrics. The extreme broad longitudinal acoustic (LA) and TA modes in $NaNbO_3$ contribute significantly to the inelastic diffuse scattering around Bragg points. The broadening of TA and TO modes are attributed to the anharmoic lattice potential in $NaNbO_3$. The coexistence of long-wavelength and zone-boundary phonon instabilities above $T_{c1}=913$ K is closely related to the complex sequence of phase transitions in $NaNbO_3$.

DOI: 10.1103/PhysRevB.80.104101 PACS number(s): 77.80.−e, 63.20.−e, 77.84.Dy

I. INTRODUCTION

A rich variety of phase diagrams in perovskite oxides ABO_3 has long been a fascinating subject of ferroelectricity. Both $KNbO_3$ and $NaNbO_3$ provide a typical example. Like $BaTiO_3$, $KNbO_3$ exhibits three ferroelectric (FE) phase transitions as a function of temperature. In contrast, $NaNbO_3$ undergoes at least six phase transitions. Figure 1 illustrates the phase diagram of $NaNbO_3$.[1] Sodium niobate $NaNbO_3$ has a simple-cubic perovskite structure above $T_{c1}=913$ K. First, the cubic ($Pm\bar{3}m$) to a tetragonal ($P4/mbm$) phase transition takes place at T_{c1}. Next, three distinct orthorhombic phases appear between $T_{c5}=643$ K and $T_{c2}=848$ K.[2] In accordance with convention,[3] the upper, middle, and lower orthorhombic phases are denoted by T_1, S, and R phases, respectively. The phase transition between the upper T_1 and middle S orthorhombic phases occurs at $T_{c3}=793$ K. The upper T_1 and middle S phases are paraelectric (PE), whereas the lower R phase between T_{c5} and $T_{c4}=753$ K is antiferroelectric (AF). Reexamination of the crystal structure shows that the T_1 orthorhombic phase has space-group $Cmcm$.[2] An AF monoclinic P phase exists in the range between $T_{c6}=193$ K and T_{c5}.[1] Finally, $NaNbO_3$ exhibits a FE rhombohedral ($R3c$) N phase below T_{c6}.[4] Unfortunately, there is still controversy about the crystal structures below T_{c3}.[1,2,5,6] More recent studies indicate that the FE rhombohedral N phase coexists the AF orthorhombic ($Pbcm$) P phase at low temperatures.[6]

High-temperature structural phase transitions in $NaNbO_3$ have been interpreted in terms of the phonon instability.[2,5,7–11] Figure 2 shows the cubic perovskite structure and its Brillouin zone. The cubic to tetragonal transition at T_{c1} was connected with the rotational instability of oxygen octahedra at the $M(0.5,0.5,0)$ point, whereas the tetragonal to orthorhombic transition at T_{c2} was related to the rotational instability at the $R(0.5,0.5,0.5)$ point. In Glazer's notation,[9] the tetragonal and T_1 orthorhombic phases are described by $[a^0a^0c^+]$ and $[a^0b^-c^+]$, respectively.[2] Inelastic neutron scattering measurements showed that the zone-boundary phonons in $NaNbO_3$ become overdamped around the cubic to tetragonal phase transition.[12] Two types of x-ray diffuse scattering were observed in $NaNbO_3$.[7,11] The diffuse scatter-

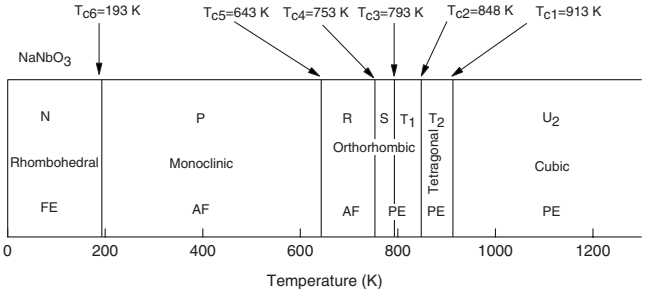

FIG. 1. The phase diagram of $NaNbO_3$ as a function of temperature. This is based on Ref. 1.

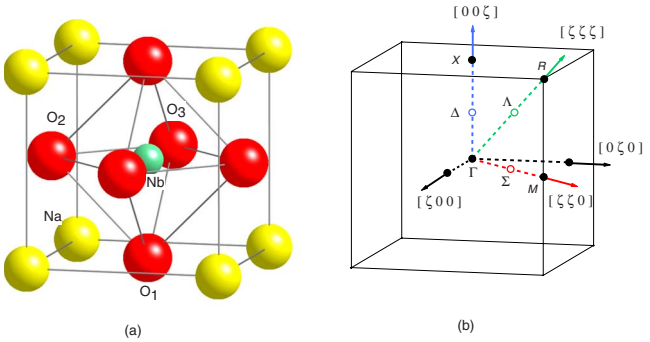

FIG. 2. (Color online) Crystal structure and Brillouin zone for cubic $NaNbO_3$. (a) In the cubic perovskite structure, the atomic positions in reduced coordinates are as follows: Na at (0,0,0), Nb at (0.5,0.5,0.5), O_1 at (0.5,0.5,0), O_2 at (0.5,0,0.5), and O_3 at (0,0.5,0.5). (b) Phonon data were collected along the Δ, Σ, and Λ directions.

ing in the $\langle 100 \rangle$ direction connecting the M and R points is explained in terms of the softening of zone-boundary phonons. The diffuse scattering in $\{100\}$ reciprocal planes is attributable to chains of Nb atoms oriented along the $\langle 100 \rangle$ directions. Infrared reflectivity measurements in cubic $NaNbO_3$ found that the frequency of zone-center transverse optic (TO) phonon decreases gradually on cooling.[13] First-principles calculations also predicted the coexistence of zone-center and zone-boundary phonon instabilities in cubic $NaNbO_3$.[14–16]

The phonon-dispersion curves for niobate counterpart, $KNbO_3$, were reported for the cubic, tetragonal, and orthorhombic phases.[17–21] Results for cubic $KNbO_3$ strongly suggest that the zone-center low-energy TO phonon is heavily damped.[17,21,22] Yu and Krakauer[23] computed the full phonon-dispersion relations for cubic $KNbO_3$ using first-principles calculations. They pointed out structural instabilities with pronounced two-dimensional character in the Brillouin zone. The motion of the Nb and O atoms plays an important role in the phase transitions of $KNbO_3$.

However, there has been no study of the phonon-dispersion relation for $NaNbO_3$. We expect that inelastic neutron scattering experiments for $NaNbO_3$ will promote a better understanding of the origin of the complicated structural phase transitions. In this paper, we present the phonon-dispersion relations for cubic $NaNbO_3$. We also report results for the inelastic diffuse scattering at high-symmetry positions. The lattice dynamics of $NaNbO_3$ is discussed in relation to those for simple perovskites and relaxor ferroelectrics.

II. EXPERIMENT

A single crystal was grown by the top-seeded solution growth method from a NaF flux. The crystal forms a dome shape and has a volume of 5 cc. The sample was covered with a series of thin Ni plates and mounted in a high-temperature furnace. The inelastic neutron scattering experiments were mainly performed using the T1–1 triple-axis spectrometer installed on the thermal guide of JRR-3M, Tokai, JAEA. Measurements in early stages were made on the 5G(PONTA) triple-axis spectrometer at JRR-3M. Incident neutron energy was fixed at 13.5 meV for the T1–1 spectrometer, and final neutron energy was fixed at 14.7 meV for the 5G spectrometer. Both constant-**Q** and constant-E scans were made. Pyrolytic graphite (PG) crystals were used as monochromator and analyzer. A PG filter was placed before the sample to remove higher-order contamination. The collimation of 40′-40′-40′-40′ was used for these spectrometers. The low-lying phonon-dispersion curves were determined along the $[\zeta,0,0](\Delta)$, $[\zeta,\zeta,0](\Sigma)$, and $[\zeta,\zeta,\zeta](\Lambda)$ high-symmetry directions. Most of the measurements were performed at 970 K, but selected phonons were also investigated up to 1230 K.

To extract the phonon peak position and its energy half-width at half maximum (HWHM) Γ, the data were fit to a Lorentzian cross section convoluted with the spectrometer resolution function using the program RESLIB.[24] We generally assumed a q-linear phonon dispersion for acoustic modes and a q-independent phonon dispersion for optic modes. For simplicity, we assumed that the dispersion for transverse acoustic (TA) Σ_3 and Λ_3 modes toward the zone-boundary point q_{ZB} is written as $E(q)=C(q-q_{ZB})$, where C is the slope. We also attempted to fit the observed data around q_{ZB} to the extended form $E(q)=E_{ZB}+C(q-q_{ZB})$, where E_{ZB} is the zone-boundary energy. Unfortunately, our attempts to obtain the reliable E_{ZB} values proved unsuccessful. For the TO Σ_4 mode in the range $0.1<\zeta<0.2$, we assumed that the dispersion is expressed as $E(q)=Dq$.

III. PHONON-DISPERSION RELATIONS

A. Zone-boundary modes

Figure 3 shows the phonon-dispersion relations for cubic $NaNbO_3$ measured at $T=970$ K($T_{c1}+57$ K). Each solid circle represents the phonon peak position, and the attached vertical bar denotes its full width at half maximum (FWHM) in energy. The solid circle with the horizontal bar shows the phonon peak position derived from the constant-E scan data using the same procedure. For the steep dispersion relation, we occasionally found the situation that the FWHM in energy is larger than the absolute value of constant-E, ΔE. For simplicity, we indicate only the vertical bar in such cases. The horizontal bar corresponds to the observed FWHM in q for the **Q**-scan peak in the constant-E condition. Table I gives the related normal modes at the high-symmetry positions for cubic $NaNbO_3$. Here we refer to the results for cubic $SrTiO_3$ tabled by Cowley.[25] The zone-boundary phonon in the TA Σ_3 branch is labeled as the M_3 mode, and that in the TA Λ_3 branch is labeled as the R_{25} mode. For the M_3 mode at $\mathbf{q}=(0.5,0.5,0)$, the rotation of octahedra along the [001] direction is in the same sense in the vertically adjacent cells, but remains in the opposite sense in the horizontally adjacent cells. For the R_{25} mode, the octahedra are rotated in the opposite sense in all adjacent cells.

The important features of the phonon dispersion are the simultaneous softening of M_3 and R_{25} phonon modes at 970 K. The softening of these modes suggests low-lying flat TA phonon-dispersion relations along the zone-boundary M-R line, although the measurements have not been performed in

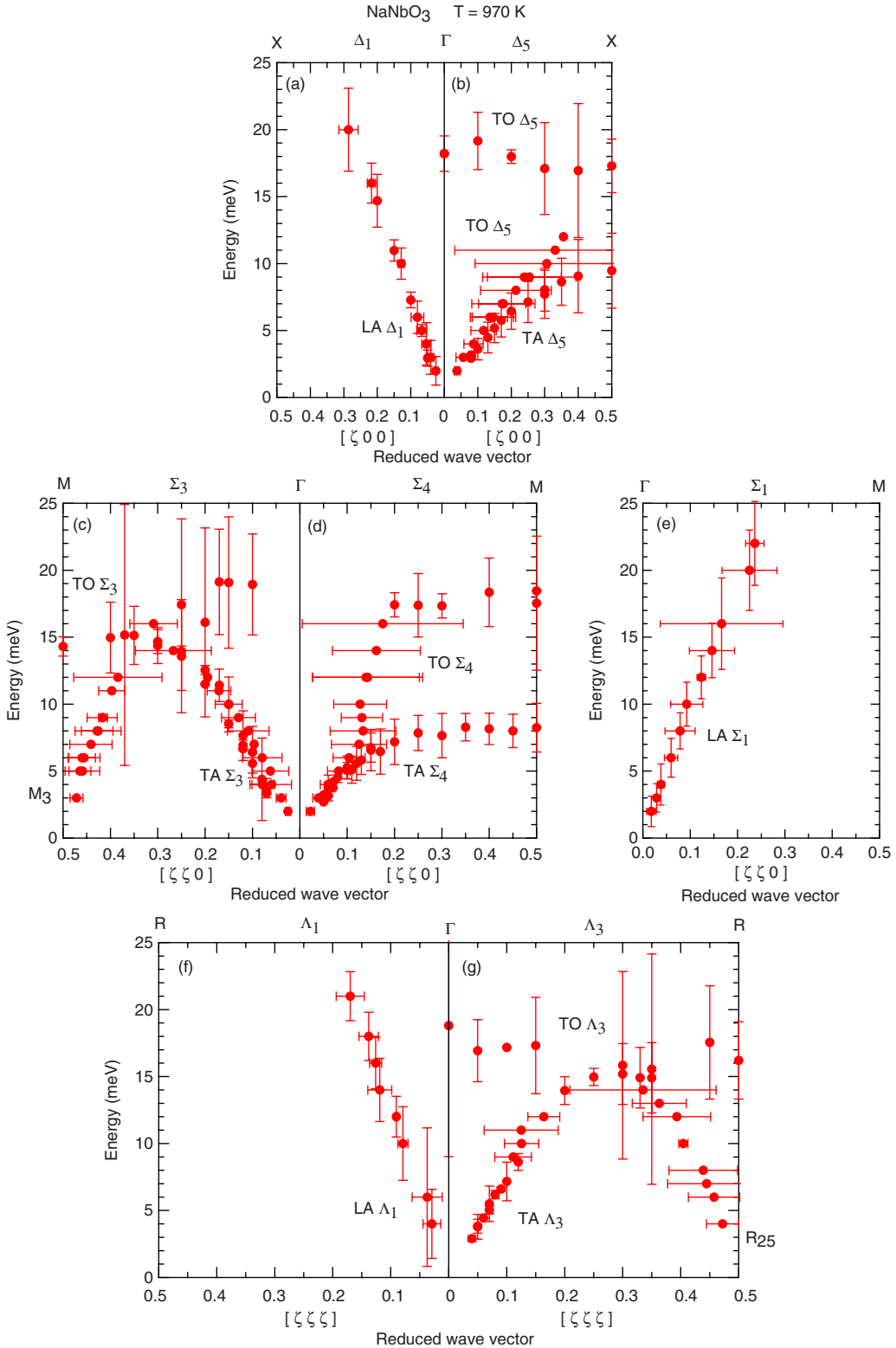

FIG. 3. (Color online) Phonon-dispersion curves for cubic $NaNbO_3$ measured at 970 K. Each solid circle and the attached vertical bar refer to the phonon peak and its FWHM, respectively. The horizontal bar denotes the observed FWHM in q for the **Q**-scan peak in the constant-E condition.

this study. In the present study, we focused on the temperature dependence of the M_3 and R_{25} modes. The inelastic-scattering intensities at $\mathbf{Q}=(1.5,1.5,0)$ polarized along the $[1\bar{1}0]$ direction were extremely lower than those at $\mathbf{Q}=(1.5,2.5,0)$. The M_3 mode at $\mathbf{Q}=(h/2,k/2,0)$ (h, k, all odd) is described as the oxygen displacement relation $O_{2x}=-O_{3y}$ (Table I). The observed intensity difference is consistent with the calculation that the inelastic structure fac-

TABLE I. Selected normal modes in $NaNbO_3$. Here we refer to the normal-mode analysis for $SrTiO_3$ given by Cowley.[25]

Point	Mode	Normal mode
$\mathbf{q}=(0,0,\epsilon),\epsilon\rightarrow 0$	Γ_{15}	Na_x, Nb_x, $O_{1x}=O_{2x}$, $O_{3x}(x\leftrightarrow y)$
$\mathbf{q}=(0,0,\zeta)$	Δ_5	Na_x, Nb_x, O_{1x}, O_{2x}, $O_{3x}(x\leftrightarrow y)$
$X(0,0,0.5)$	X_5	Nb_x, O_{2x}, $O_{3x}(x\leftrightarrow y)$
	X_5'	Na_x, $O_{1x}(x\leftrightarrow y)$
$\mathbf{q}=(\zeta,\zeta,0)$	Σ_3	$Na_x=-Na_y$, $Nb_x=-Nb_y$, $O_{1x}=-O_{1y}$, $O_{2x}=-O_{3y}$, $O_{3x}=-O_{2y}$
	Σ_4	Na_z, Nb_z, O_{1z}, $O_{2z}=O_{3z}$
$M(0.5,0.5,0)$	M_2'	Na_z
	M_3	$O_{2x}=-O_{3y}$
	M_3'	Nb_z, O_{1z}
	M_5'	Na_x, Nb_y, $O_{1y}(x\leftrightarrow y)$
$R(0.5,0.5,0.5)$	R_{25}	$O_{1y}=-O_{2z}$
		$O_{1x}=-O_{3z}$
		$O_{2x}=-O_{3y}$
	R_{15}	Na_x, $O_{1y}=O_{2z}$

tor $F(\mathbf{Q})$ for the M_3 mode at $\mathbf{Q}=(h/2,k/2,0)$ (h, k, all odd) is zero with $h=k$. Figures 4(a) and 4(b) plot the constant-$\mathbf{Q}$ scans at $\mathbf{Q}=(1.5,2.5,0)$ with polarization along the $[1\bar{1}0]$ direction determined at $T=970$, 1080, and 1230 K. Constant-$\mathbf{Q}$ scan measurements at 970 and 1080 K indicate that the diffuse scattering at the $M(0.5,0.5,0)$ point increases dramatically with decreasing the energy ΔE. In contrast, constant-$\mathbf{Q}$ scan measurements at 1230 K show that the diffuse scattering below $\Delta E=2$ meV is considerably suppressed. Furthermore, a broad peak emerges around $\Delta E=3$ meV at 1230 K, as shown in Fig. 4(b). These results indicate that the M_3 mode energy increases gradually with increasing temperature. The inelastic diffuse scattering at the $M(0.5,0.5,0)$ point polarized along the $[1\bar{1}0]$ direction remains up to $\Delta E=9$ meV in the range between 970 and 1230 K. It would be difficult to estimate the intrinsic broad peak position observed at 1230 K without the knowledge of the E dependent background.

For comparison, we performed the constant-$\mathbf{Q}$ scans at $\mathbf{Q}=(-0.5,-0.5,2)$ polarized along the [001] direction at 970

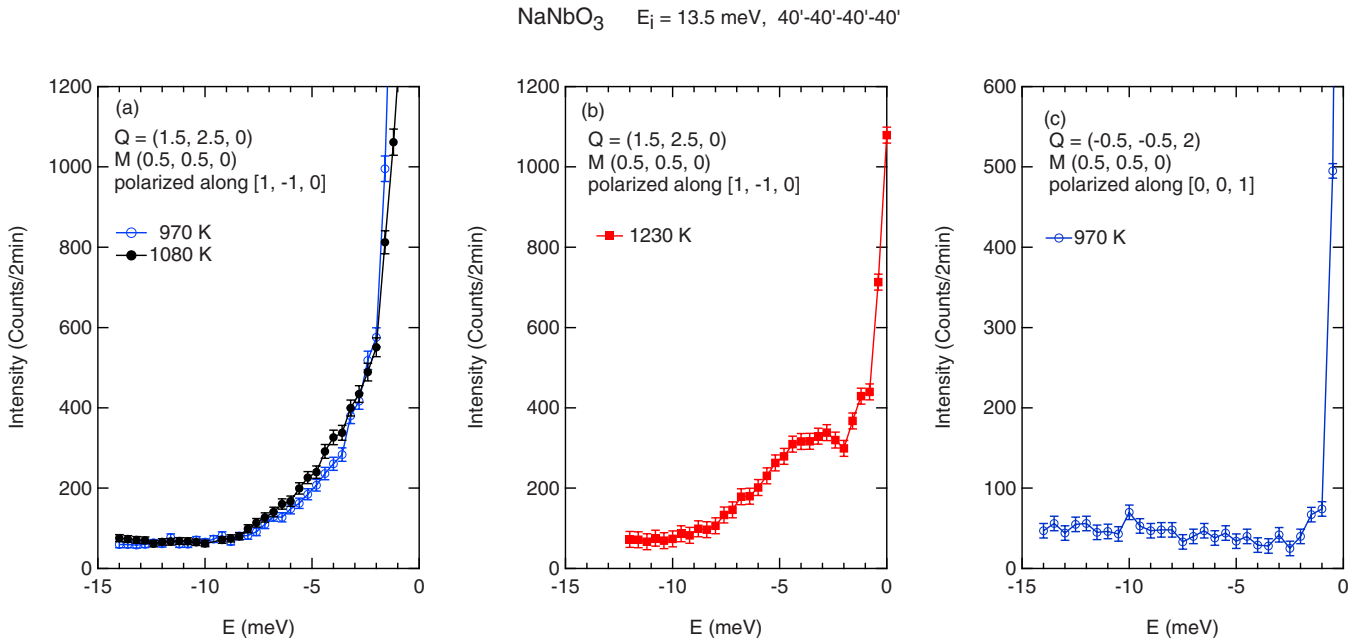

FIG. 4. (Color online) Constant-$\mathbf{Q}$ scans in $NaNbO_3$ at the M point. (a)–(b) the scans at the $M(0.5,0.5,0)$ point polarized along the $[1\bar{1}0]$ direction measured at 970, 1080, and 1230 K. (c) the scan at the $M(0.5,0.5,0)$ point polarized along the [001] direction measured at 970 K. The lines are guides to the eye.

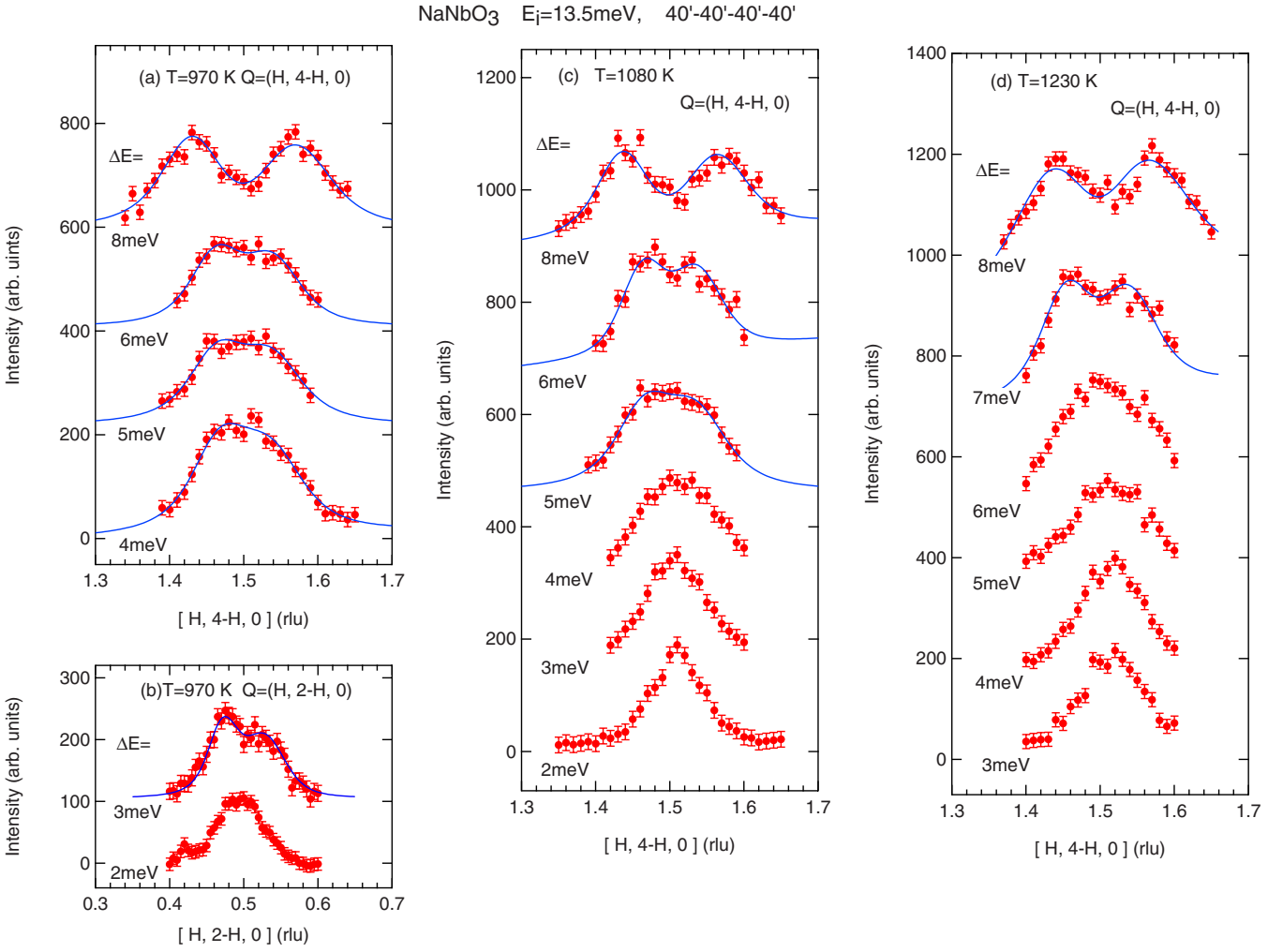

FIG. 5. (Color online) Constant-E scans in $NaNbO_3$ for the Σ_3 mode through the M point measured at (a)–(b)T=970, (c)1080, and (d)1230 K. Solid lines are fits to the data as described in the text.

K. We assign the phonons determined in this configuration as the M_3' mode, in light of the normal-mode analysis for $KTaO_3$.[26] As indicated in Table I, the M_3' mode at $\mathbf{q}=(0.5,0.5,0)$ corresponds to the motion of the O_1 and Nb atoms along the [001] direction. Thus the inelastic structure factor $F(\mathbf{Q})$ for the M_3' mode at $\mathbf{Q}=(h/2,k/2,0)$ (h, k, all odd) is finite with $h=k$. Figure 4(c) shows that the inelastic diffuse scattering at the $M(0.5,0.5,0)$ point polarized along the [001] direction is suppressed except for a narrow range below 1 meV. As shown in Fig. 3, the flat TA Σ_4 branch has an energy of 8.2 ± 1.1 meV toward the M point. Different polarization dependence clearly shows that the dynamic rotation of the oxygen octahedra gives rise to the inelastic diffuse scattering at the M point polarized along the $[1\bar{1}0]$ direction.

Figure 5 shows representative constant-E scans for the Σ_3 mode through the M point determined at T=970, 1080, and 1230 K. Solid lines in Fig. 5 are fits to the double-peak structure in constant-E scans. The TA Σ_3 curve at 970 K is plotted in Fig. 3(c), based on these fits. The data analysis also shows that typical FWHM of the TA Σ_3 phonon peak at T =970 K is 3.5 meV for ΔE=3 meV and 6.8 meV for ΔE =5 meV. The raw data determined at T=970 K exhibits two peaks for ΔE=3 meV, whereas the data for ΔE=2 meV shows a single peak. In light of these results, the broadened M_3 phonon mode at 970 K is overdamped and its peak is dominantly distributed up to 2 meV. The high-energy tail up to 9 meV at $\mathbf{Q}=(1.5,2.5,0)$ in Fig. 4 appears to be connected with a pair of the steep downward TA Σ_3 phonon branches toward the M point. As shown in Figs. 5(c) and 5(d), the peak separation in the raw data starts at ΔE=5 meV at 1080 K and 7 meV at 1230 K. Furthermore, the peak width at ΔE=4 meV decreases with increasing temperature. The combination of constant-E and constant-$\mathbf{Q}$ results shows that the low-energy M_3 mode exhibits an extremely gradual softening with decreasing temperature toward T_{c1}=913 K.

Figure 6 shows a series of constant-E scans for the Λ_3 mode through the R point measured at T=970 and 1170 K. The constant-E data shows the double-peak structure at 970 K above ΔE=4 meV, and at 1170 K above ΔE=5 meV. Below these energies the single peak is found in the constant-E scans. The typical FWHM of the TA Λ_3 phonon peak at T=970 K is 5.7 meV for ΔE=4 meV and 7.4 meV for ΔE=6 meV. Constant-$\mathbf{Q}$ scans at $\mathbf{Q}=(0.5,0.5,1.5)$ performed at T=970 and 1170 K are shown in Fig. 6(c). The intensities at $\mathbf{Q}=(0.5,0.5,1.5)$ increases significantly with

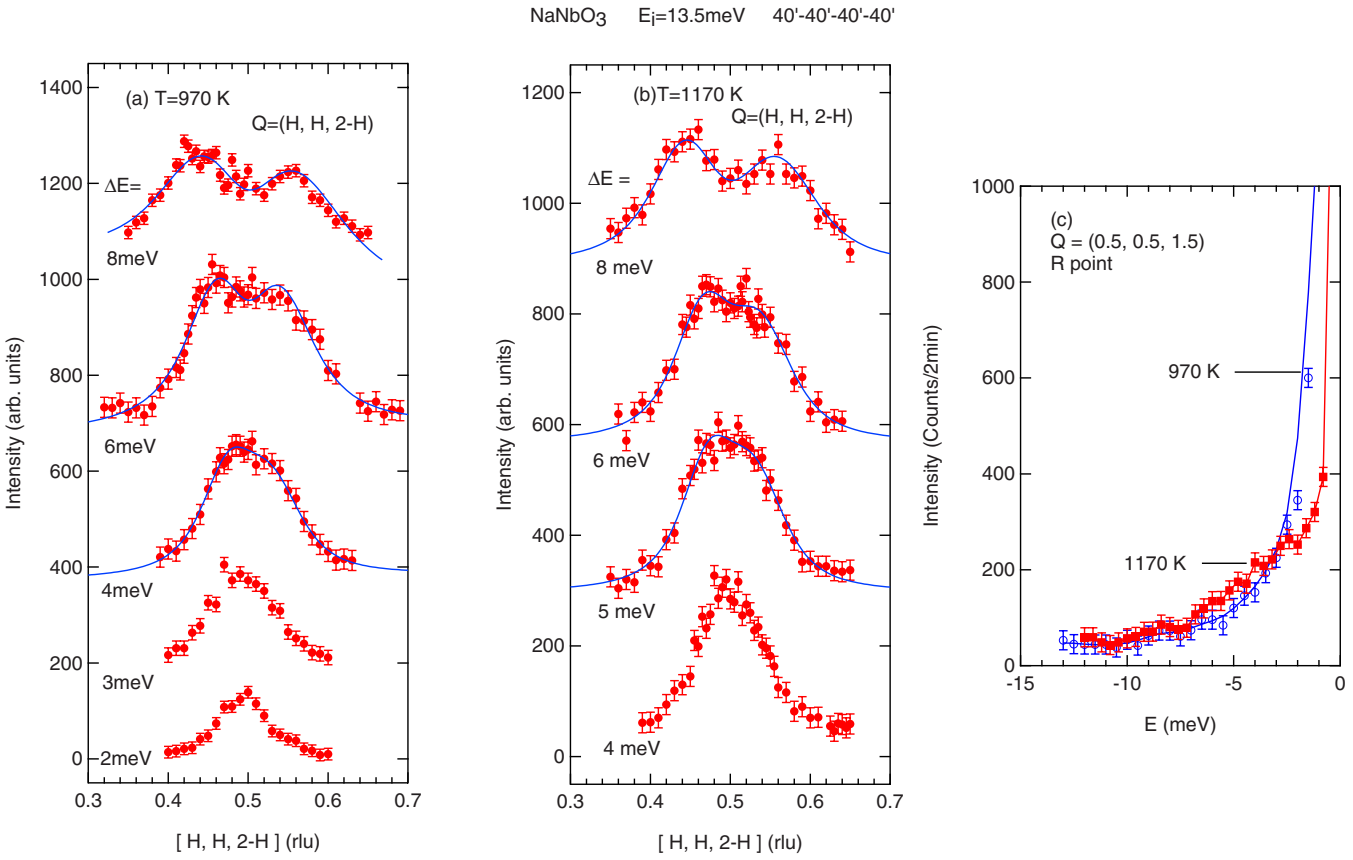

FIG. 6. (Color online) Constant-E scans for the Λ_3 mode through the R point and constant-**Q** scans at the R point in $NaNbO_3$. (a) Constant-E scans measured at 970 K. (b) Constant-E scans measured at 1170 K. (c) Constant-**Q** scans measured at 970 and 1170 K. Solid lines in (a) and (b) are fits to the data. Solid lines in (c) are guides to the eye.

decreasing energy ΔE. As shown in Fig. 6(c), the intensities in the range $\Delta E \leq 3$ meV decrease with increasing temperature. Furthermore, the intensities around $\Delta E=5$ meV at $T=1170$ K are slightly higher than those at $T=970$ K. Thus the R_{25} mode in cubic $NaNbO_3$ also shows an extremely gradual softening with decreasing temperature. Like the M_3 mode, the R_{25} mode at 970 K appears to be overdamped. The combination of constant-E and constant-**Q** data suggests that the peak of R_{25} mode at 970 K is mainly distributed up to 3 meV.

On the basis of geometrical considerations, the successive phase transitions at $T_{c1}=913$ K, and $T_{c2}=848$ K were associated with the condensation of M_3, and R_{25} modes, respectively.[2,5,8–11] X-ray diffuse scattering around the M point is critical in the vicinity of T_{c1},[7,11] whereas x-ray diffuse scattering around the R point is critical in the vicinity of T_{c2}.[11] The present study confirms the simultaneous softening of these zone-boundary modes in cubic $NaNbO_3$. The simultaneous softening is partly because these modes are weakly temperature dependent, and because the tetragonal phase exists in a relatively narrow temperature range between $T_{c2}=0.93T_{c1}$ and T_{c1}. The simultaneous softening of M_3 and R_{25} modes at the same frequency suggests a weak coupling between the oxygen motions in different layers, because the sense of rotations is opposite along the [001] direction between these zone-boundary modes. From the x-ray diffuse linewidth, Denoyer *et al.*[7] deduced that an order of magnitude for the planar disorder is 400 Å in cubic $NaNbO_3$. They proposed a model that the rotations of the octahedra are coherent within a microdomain above T_{c1}. The broad energy distribution of M_3 and R_{25} modes in Figs. 4–6 appears to have a close connection with the low-lying flat M-R phonon branch.

The temperature-dependent parts in the TA Σ_3 and TA Λ_3 branches are confined to small regions around the M and R points, respectively. A series of constant-E scans reveals that the negative slope of the TA Σ_3 curve toward the M point is almost temperature independent in the energy range 7 to 12 meV. As shown in Fig. 5, the peak positions measured at $\Delta E=8$ meV are temperature independent between 970 and 1230 K. The TA Λ_3 curve toward the R point is also temperature independent in the range 6 to 10 meV. These results reflect the rigidity of the oxygen octahedron.

B. Comparison with zone-boundary modes in ABO_3

Systematic first-principles calculations predicted that the R_{25} phonon instabilities exist in six cubic perovskites $BaZrO_3$, $PbTiO_3$, $SrTiO_3$, $NaNbO_3$, $PbZrO_3$, and $CaTiO_3$.[15] Unfortunately, there is no experimental phonon-dispersion data for $BaZrO_3$, $PbZrO_3$, and $CaTiO_3$. Our experimental findings support the first-principles calculations that the R_{25} phonon mode in $NaNbO_3$ is strongly unstable.[14–16] Strontium titanate $SrTiO_3$ undergoes a structural phase transition at $T_0=105$ K. Shirane and Yamada[27] revealed the softening of R_{25}

TABLE II. Zone-boundary TA phonon energies (meV) for several perovskite oxides.

	X	$M(0.5,0.5,0)$ polarized along [001]	$M(0.5,0.5,0)$ polarized along $[1\bar{1}0]$	R
$NaNbO_3$ [a]	9.5 ± 2.8	8.2 ± 1.8	~0 to ~2	~0 to ~3
$KNbO_3$ [b]	7.7		19.6	
$KNbO_3$ [c]		7		18.6
$KTaO_3$ [d]	7.4	6.8	20.4	22
$BaTiO_3$ [e]	14.3	14.2	14.2	17.1
$SrTiO_3$ [f]	14.7	10.9		6.4
$SrTiO_3$ [g]			8.4	2
$PbTiO_3$ [h]	8.1 ± 0.1	8.34 ± 0.05	8.0 ± 0.1	

[a]Present work measured at $970(T_{c1}+57)$ K.
[b]Reference 18. Measured in the tetragonal phase between 488 and 708 K.
[c]Reference 20. Measured at room temperature in the orthorhombic phase.
[d]Reference 31. Measured at 300 K.
[e]Reference 32. Measured at 423 K.
[f]Reference 33. Measured at 297 K.
[g]Reference 27. Measured at $120(T_c+15)$ K.
[h]Reference 29. Measured at room temperature in the tetragonal phase.

phonon mode in cubic $SrTiO_3$. For $SrTiO_3$, the R_{25} phonon energy is lower than 2 meV at 120 K (T_0+15 K), whereas the M_3 phonon energy is 8 meV.[27] Moreover, the intrinsic linewidth of the R_{25} mode is estimated to be 0.6 meV at 112 K. The broadened R_{25} mode found in $NaNbO_3$ is in sharply contrast with the well-defined R_{25} mode in $SrTiO_3$. For $SrTiO_3$ the softening of the well-defined R_{25} mode indicates that a strong coupling exists between the oxygen motions in adjacent octahedron layers. In contrast, the low-lying flat M_3-R_{25} branch in $NaNbO_3$ suggests a weak coupling between the oxygen motions in adjacent layers. The unstable flat M_3-R_{25} branch is also computed for $PbZrO_3$.[28] For tetragonal $PbTiO_3$, the phonon-dispersion curves show the absence of the zone-boundary-phonon softening,[29] although a weak R_{25} phonon instability is predicted for cubic $PbTiO_3$.[15,28]

For niobate counterpart, $KNbO_3$, neutron inelastic-scattering experiments show the stability of the zone-boundary phonon modes.[17–21] First-principles studies in $KNbO_3$ also confirm the stable zone-boundary phonon modes.[15,23] Zhong and Vanderbilt[15] found that the ionic radius ratio in ABO_3 is sensitive to the R-point instability. Lattice instabilities in ABO_3 are described in terms of a tolerance factor $t=(r_A+r_O)/\sqrt{2}(r_B+r_O)$, where r_A, r_B, and r_O are the A, B, and oxygen ionic radii, respectively. The tolerance factors t are 0.97 for $NaNbO_3$ and 1.06 for $KNbO_3$.[30] A smaller Na atom enhances the possibility of the octahedron rotation in $NaNbO_3$, whereas a larger K atom prohibits the low-energy rotational motion in $KNbO_3$.

The zone-boundary phonon frequencies for $NaNbO_3$ are compared in Table II with those for several perovskite oxides. The zone-boundary TA phonon energies and eigenvec-

TABLE III. Elastic constants C_{ij} (10^{11} N/m^2) for several perovskite oxides.

	C_{11}		C_{12}		C_{44}	
	Expt.	Calc.[g]	Expt.	Calc.[g]	Expt.	Calc.[g]
$NaNbO_3$	2.3 ± 0.05 [a]	4.47	0.9 ± 0.2 [a]	0.86	0.76 ± 0.01 [a]	0.71
$KNbO_3$	2.32 ± 0.05 [b]	4.70	0.9 ± 0.1 [b]	0.73	0.756 ± 0.015 [b]	1.03
$KTaO_3$	3.936[c]				1.071[c]	
$BaTiO_3$	2.11 ± 0.06 [d]	3.23	1.07 ± 0.05 [d]	1.26	0.562 ± 0.017 [d]	1.25
$SrTiO_3$	3.17[e]	3.78	1.02[e]	1.14	1.23[e]	1.17
$PbTiO_3$	2.37 ± 0.03 [f]	3.41	0.90 ± 0.05 [f]	1.38	0.69 ± 0.01 [f]	1.04

[a]Present work measured at 970 K.
[b]Reference 34. Brillouin scattering measured at room temperature in the orthorhombic phase.
[c]Reference 35. Ultrasonic velocity measured at 300 K.
[d]Reference 36. Brillouin scattering measured at room temperature in the tetragonal phase.
[e]Reference 37. Ultrasonic velocity measured at 300 K.
[f]Reference 38. Brillouin scattering measured at room temperature in the tetragonal phase.
[g]Reference 39. Computed for the cubic phase.

tors were calculated for $KTaO_3$,[26] and $KNbO_3$.[23] In light of these calculations, we assign the TA Δ_5 mode at the $X(0.5,0,0)$ point as X_5. As indicated in Table I, the X_5 mode at (0,0,0.5) consists of the transverse motion of the Nb, O_2, and O_3 atoms. Based on the analyses of $KNbO_3$ (Ref. 23) and $KTaO_3$,[26] we interpret that the TA M_3' and TA X_5 modes in $NaNbO_3$ are dominated by the Nb atom motion. As shown in Fig. 3, the TA Σ_4 mode for $NaNbO_3$ exhibits a flat dispersion between [0.2,0.2,0] and [0.5,0.5,0]. Similar flat dispersion relations along the [101] directions are found for orthorhombic $KNbO_3$,[20] and cubic $KTaO_3$.[31] The low-energy rotational M_3 mode in $NaNbO_3$ exhibits a sharp contrast to the K atom dominated M_5' modes in $KTaO_3$ and $KNbO_3$.[23,26] Furthermore, there is an obvious difference in the zone-boundary normal modes between $NaNbO_3$ and $BaTiO_3$.[28] The energy of the TA X_5 mode for $NaNbO_3$ is lower than that of the Ba-atom dominated X_5' mode for $BaTiO_3$, and the energy of the TA M_3' for $NaNbO_3$ is lower than that of the Ba-atom dominated M_5' mode for $BaTiO_3$.[28]

C. Elastic constants

The elastic constants C_{ij} for cubic $NaNbO_3$ were consistently deduced from a set of the initial slopes for acoustic-phonon branches around $\mathbf{q}=0$. The extreme broadening of acoustic phonons creates uncertainty about C_{ij} values. The details of the broadening will be given in Sec. III D. The present C_{ij} values for $NaNbO_3$ are compared in Table III with those for $KNbO_3$, $KTaO_3$, $BaTiO_3$, and $PbTiO_3$. The measured C_{ij} values for $NaNbO_3$ are approximately equal to the corresponding values for $KNbO_3$.[34] The first-principles calculation revealed that the Born effective charges for $NaNbO_3$ are remarkably similar to those for $KNbO_3$.[14] The Na and K atoms have an ionic character in these niobates. The anomalously large Born effective charges for Nb atoms indicate the large covalent interaction between the Nb and O atoms. The relative atomic mass M are 163.89 for $NaNbO_3$ and 180.01 for $KNbO_3$. The difference in the A-site mass will have a limited influence on the C_{ij} values. Thus the similarity of elastic constants between $NaNbO_3$ and $KNbO_3$ is mainly due to the similar electronic structures. As listed in Table III, the experimental C_{11} and C_{44} values for $KTaO_3$ are considerably higher than the corresponding values for Nb- and Ti-based perovskites.

In the 1990s, King-Smith and Vanderbilt[40] performed systematic first-principles calculations for the structural and dy-

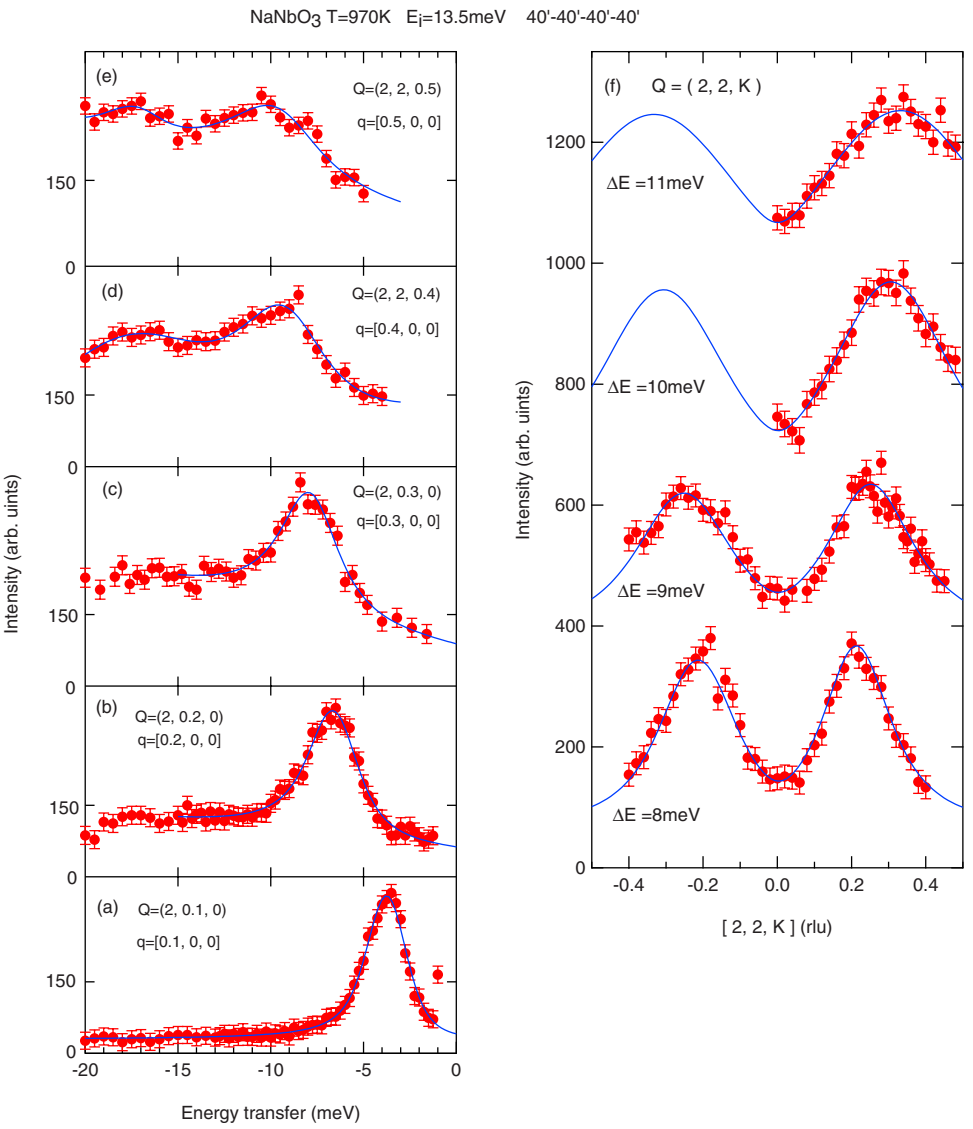

FIG. 7. (Color online) (a)–(e) Constant-**Q** scans in $NaNbO_3$ for the TA Δ_5 and TO Δ_5 modes. (f) Constant-E scans in $NaNbO_3$ along the [100] direction. Solid lines are fits to the data.

namical properties of cubic perovskites including $NaNbO_3$, $KNbO_3$, $BaTiO_3$, $SrTiO_3$, and $PbTiO_3$. They calculated the elastic constants expressed in energy units, B_{ij}, and the lattice-constant a. The elastic constant C_{ij} is expressed as B_{ij}/a^3. The calculated C_{ij} values given in Table III are obtained from the revised first-principles calculation results of Díeguez *et al.*[39] The calculated C_{12} and C_{44} values for $NaNbO_3$ are in good agreement with the experimental values. In contrast, the theoretical C_{11} values for $NaNbO_3$ and $KNbO_3$ are approximately twice as large as the experimental values. King-Smith and Vanderbilt[40] predicted that $NaNbO_3$ and $KNbO_3$ have larger values of B_{11} than $BaTiO_3$ and $PbTiO_3$. Generally first-principles calculations overestimate the elastic constant C_{11} for ABO_3.[41]

D. TA and TO phonons near the zone center

1. Δ_5 mode

A complicated situation was observed for the TA Δ_5, and $TO_1\Delta_5$ phonon branches along the $[\zeta,0,0]$ direction. Figure 7 shows representative constant-**Q** and constant-E scans for the transverse Δ_5 modes. A series of constant-**Q** scans for $|\mathbf{q}| \geq 0.25$ exhibits the unusually high background on the high-energy $|\Delta E|$ side of the TA Δ_5 phonon peak. Furthermore, the phonon peak positions determined from the analysis of constant-E scans deviate systematically from those from constant-**Q** scans. These results suggest that the $TO_1\Delta_5$ mode energy is slightly higher than the TA Δ_5 mode energy. Figure 3(b) indicates the possibility that the TA Δ_5 phonon overlaps gradually with the $TO_1\Delta_5$ phonon with decreasing $|\mathbf{q}|$ in the $[\zeta,0,0]$ direction. The results imply that the soft TO_1 mode couples to the TA mode. In cubic perovskite, a lowest-order interaction should be linear in strain and quadratic in polarization. The analysis of constant-**Q** scans shows that the FWHM of the Δ_5 phonon peak is 1.6 meV at $\mathbf{q}=[0.1,0,0]$ and 3.5 meV at $\mathbf{q}=[0.2,0,0]$. These peak widths of the Δ_5 mode for $NaNbO_3$ are much larger than the corresponding widths for $PbTiO_3$.[29] The broadening of the Δ_5 modes near the zone center is mainly attributed to the anharmonic lattice potential in $NaNbO_3$. The overlap between TA Δ_5 and $TO_1\Delta_5$ phonon modes is also found in cubic $KNbO_3$.[21] The close relationship of these Δ_5 modes in $NaNbO_3$ differ significantly from an anticrossing between TA and TO phonon branches in the [100] direction found for $KTaO_3$.[42] For $KTaO_3$ the softening of the TO phonon mode reduces the TA phonon frequencies in a wide region slightly apart from the zone center.

2. Σ_4 mode

The $TO_1\Sigma_4$ phonon branch drops sharply near $\mathbf{q}=[0.15,0.15,0]$, and then merges into the TA Σ_4 phonon branch at $\mathbf{q}_c=[0.12,0.12,0]$, as shown in Fig. 3. Below $\mathbf{q}_c$, our attempts to find the distinct $TO_1\Sigma_4$ mode were unsuccessful. The $TO_1\Sigma_4$ phonon appears to be coupled with the TA Σ_4 phonon below $\mathbf{q}_c$. Figure 8 shows a series of constant-E scans along the $[\zeta,\zeta,0]$ direction measured at 970 and 1170 K. Solid lines are fit to the data. The typical FWHM of the $TO_1\Sigma_4$ phonon is 8.8 meV at $|\Delta E|=8$ meV and 970 K. It is not surprising that we were unable to detect such a steep slope using the constant-**Q** method. The results

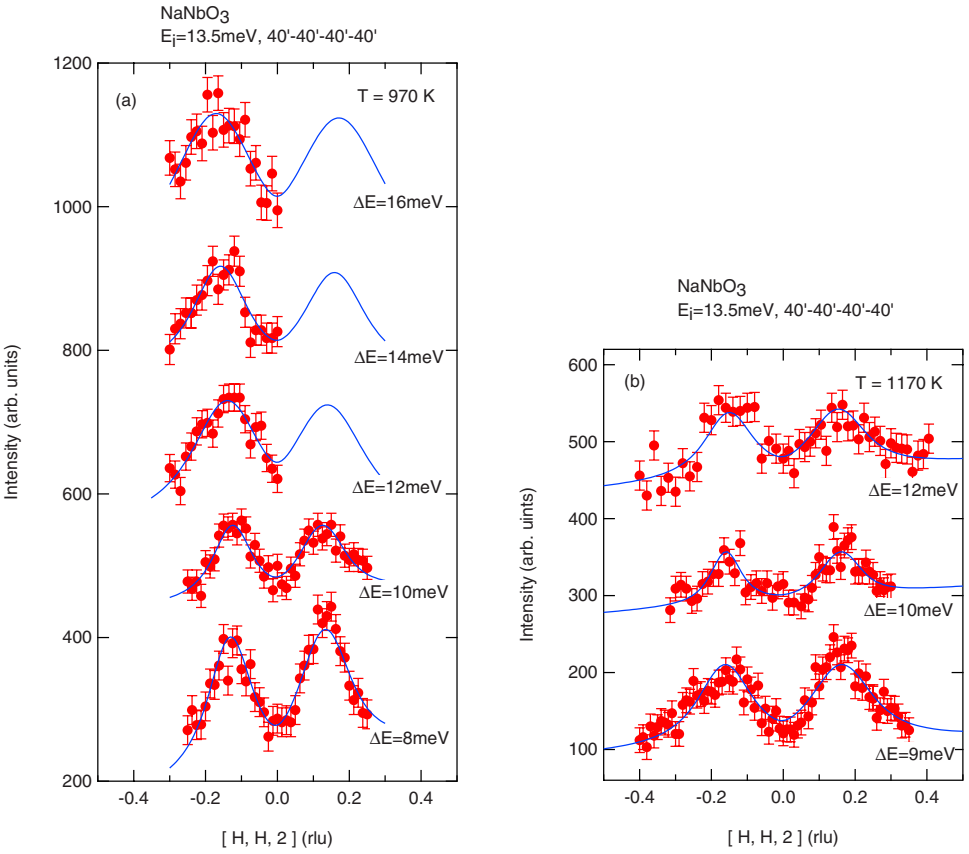

FIG. 8. (Color online) Constant-E scans in $NaNbO_3$ for the $TO_1\Sigma_4$ mode measured at (a) $T=970$ K and (b) 1170 K. Solid lines are fits to the data.

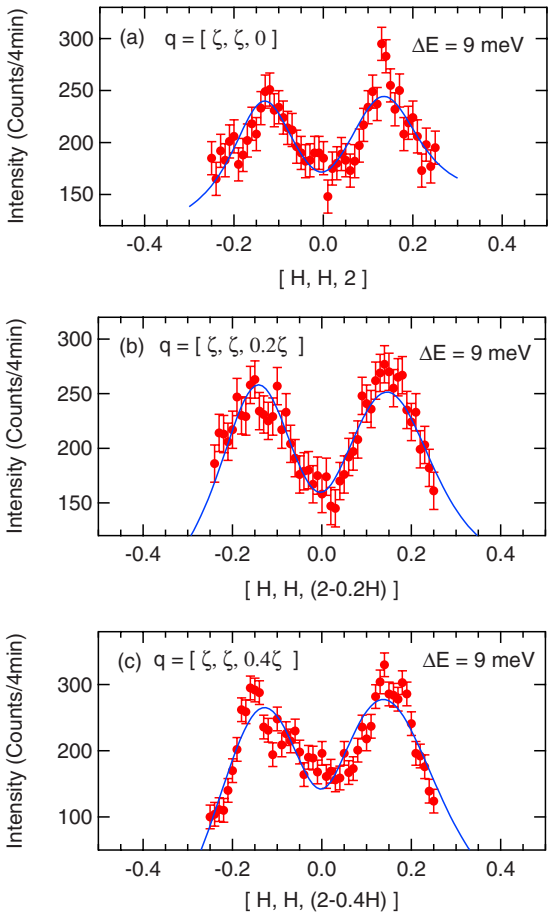

FIG. 9. (Color online) Constant-E scans in $NaNbO_3$ measured at $T=970$ K along (a) the $[\zeta,\zeta,0]$, (b) $[\zeta,\zeta,0.2\zeta]$, and (c) $[\zeta,\zeta,0.4\zeta]$ directions. Solid lines are fits to the data.

for constant-E scans indicate that the steep slope near $\mathbf{q}=[0.15,0.15,0]$ is temperature independent up to 1170 K. Figure 9 shows a set of constant-E scans for $\Delta E=9$ meV performed at 970 K along the $[\zeta,\zeta,0]$, $[\zeta,\zeta,0.2\zeta]$, and $[\zeta,\zeta,0.4\zeta]$ directions. These data suggest that the steep slope of the TO phonon branches remains along the $[\zeta,\zeta,0.2\zeta]$, and $[\zeta,\zeta,0.4\zeta]$ directions.

A possible explanation for the steep drop in the $TO_1\Sigma_4$ branch is the precursor to the softening of zone-center TO_1 mode. The ground state of $NaNbO_3$ is the FE phase below $T_{c6}=193$ K. Moreover, first-principles calculations predicted the softening of the zone-center TO_1 mode for $NaNbO_3$.[14–16] Another possible explanation for the steep slope is the phonon instability associated with the upper T_1 to middle S orthorhombic phase transition at $T_{c3}=793$ K or the middle S to lower R orthorhombic phase transition at $T_{c4}=753$ K. For the T_1 orthorhombic phase, the lattice parameters a, b, and c are given by $a\approx 2a_0$, $b\approx 2a_0$, and $c\approx 2a_0$, where a_0 is the lattice parameter for the cubic phase.[3,5] For the S orthorhombic phase, the lattice parameters a, b, and c are written as $a\approx 2a_0$, $b\approx 4a_0$, and $c\approx 6a_0$.[1] The lower R orthorhombic phase is AF between $T_{c5}=643$ K and T_{c4}. The lattice parameter for the R phase is also expressed as $a\approx 2a_0$, $b\approx 4a_0$, and $c\approx 6a_0$.[1] It seems likely that the anomalous $TO_1\Sigma_4$ mode near $\mathbf{q}_c=[0.12,0.12,0]$ would be correlated with the combination of the twofold, fourfold, and sixfold periodicities in the S and R phases. At present, the origin of the fourfold and sixfold periodicity in the S and R phases is not well understood. First-principles calculations for $NaNbO_3$ predict the existence of one orthorhombic phase.[16] The calculations also show that the orthorhombic phase is not very stable. Further research is needed to understand the existence of AFE and FE phases in $NaNbO_3$.

The steep drop in the $TO_1\Sigma_4$ branch for $NaNbO_3$ is basically similar to the so-called "phonon waterfall" observed for the following relaxor ferroelectrics: $PbZn_{1/3}Nb_{2/3}O_3$(PZN),[43,44] $PbMg_{1/3}Nb_{2/3}O_3$(PMN),[45] $(1-x)PbZn_{1/3}Nb_{2/3}O_3-xPbTiO_3$ (PZN-PT),[46,47] and $(1-x)PbMg_{1/3}Nb_{2/3}O_3-xPbTiO_3$ (PMN-PT).[48,49] For the Pb-based relaxors, the TO-phonon waterfall occurs at a reduced wave-vector $q_{wf}\sim 0.13$. The interpretation of the phonon waterfall in relaxors is still controversial.[47,49] Gehring *et al.*[46] interpreted that the characteristic wave-vector q_{wf} corresponds to the size of polar nanoregions (~30 Å) in relaxors. Unlike the Pb-based relaxors, cubic $NaNbO_3$ is entirely free from the atomic and charge disorder at the B site. For cubic $NaNbO_3$, the characteristic wave-vector value $|\mathbf{q}_c|\sim 0.17$ r.l.u. is much larger than $2\pi/L\sim 0.01$ r.l.u., where L is the average size of two-dimensional microdomains (~400 Å).[7] Thus the existence of microdomains in $NaNbO_3$ has no influence on the steep drop in the $TO_1\Sigma_4$ branch. The similar TO-phonon behavior in $NaNbO_3$ strongly suggests that the TO phonon waterfall in relaxors is independent of the size of polar nanoregions. For relaxor perovskites, Hlinka *et al.*[47] interpreted the phonon waterfall in terms of a damped harmonic-oscillator model in the presence of the TA and TO phonon coupling. Their model appears applicable to the behavior of the TA Σ_4 and $TO_1\Sigma_4$ branches in $NaNbO_3$.

3. Inelastic diffuse scattering

Figure 10 shows constant-$\mathbf{Q}$ scans at $\mathbf{Q}=(2,2,0)$ determined at $T=970$ and 1180 K. The inelastic diffuse scattering at the zone center exists up to 10 meV and is essentially temperature independent. A series of constant-$\mathbf{Q}$ scans at $\mathbf{Q}=(H,2,0)$ for small H is plotted in Fig. 10. Constant-E scans across $\mathbf{Q}=(0,2,0)$ were also performed for the LA and TA modes. For example, constant-E scans at $\Delta E=4$ meV show that the intensities at $\mathbf{Q}=(0,2,0)$ are higher than the background outside a pair of acoustic-phonon peaks. Constant-E scans at $\Delta E=2$ meV indicate that the diffuse scattering around (0,2,0) is elongated along the [100] direction, perpendicular to the scattering vector $\mathbf{Q}=(0,2,0)$. These results clearly show that the inelastic diffuse scattering at the zone center mainly originates from the extremely broad TA and LA modes.

X-ray diffuse scattering in {100} reciprocal planes was reported in cubic $NaNbO_3$.[7,11] Present results strongly suggest that the broad LA and TA phonons dominate the two-dimensional x-ray diffuse scattering in $NaNbO_3$. Similar x-ray diffuse scattering was observed in cubic $KNbO_3$ and $BaTiO_3$.[50–52] However, the origin of x-ray diffuse scattering in cubic ABO_3 is still controversial.[50–55] X-ray-absorption fine-structure (XAFS) studies for cubic $NaNbO_3$ and $KNbO_3$ showed that the Nb atom is located at off-center

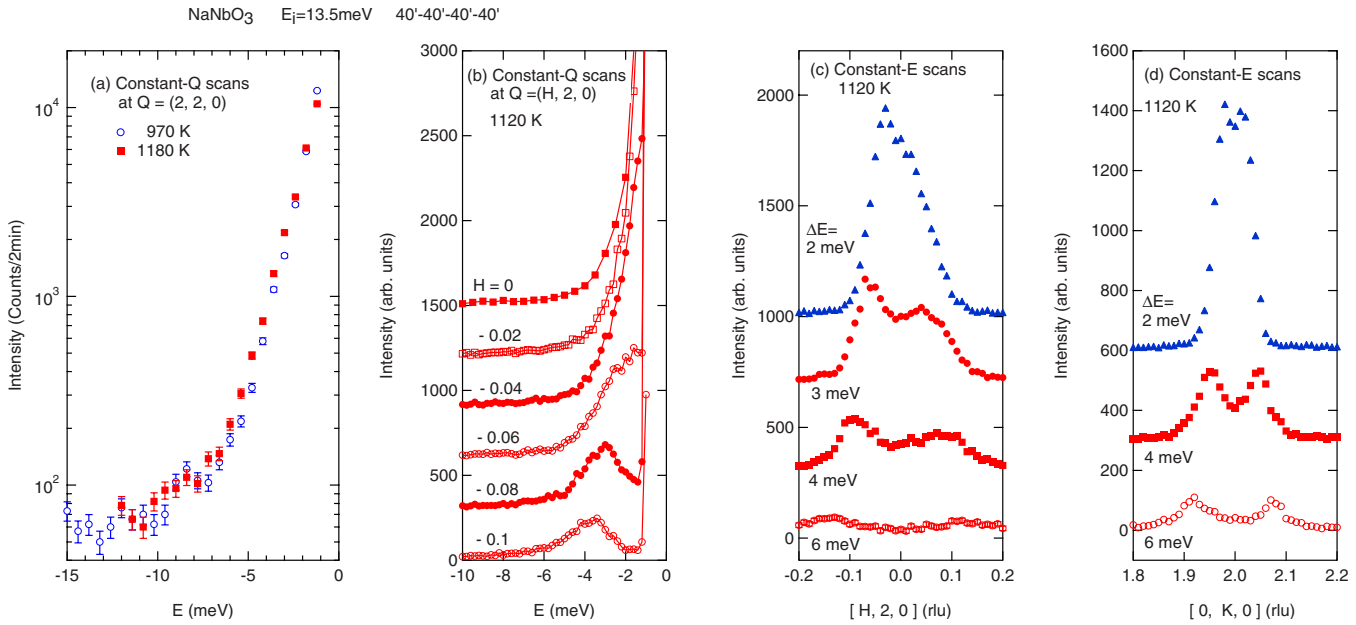

FIG. 10. (Color online) Constant-**Q** and constant-E scans around the zone center in $NaNbO_3$. (a) Constant-**Q** scans at $\mathbf{Q}=(2,2,0)$ measured at 970 and 1180 K. (b) A series of constant-**Q** scans at $\mathbf{Q}=(H,2,0)$. (c) Constant-E scans along the [H,2,0] direction. (d) Constant-E scans along the [0,H,0] direction.

positions.[56–58] The local displacement of the Nb atom reflects an anharmonic lattice potential in cubic $NaNbO_3$. In contrast, synchrotron x-ray studies for cubic $KNbO_3$ and $BaTiO_3$ suggested that the distribution of x-ray diffuse scattering intensities is attributed to the low-frequency phonon branches.[52,53]

4. TO_2 *mode*

Figure 3 shows that higher-energy $TO_2\Delta_5$, Σ_3, and Λ_3 modes are weakly q dependent. The zone-center TO_2 phonon energy is approximately 18 meV, whereas the TO phonon energy determined using infrared reflectivity is 11 meV at T_{c1}.[13] The reason for this discrepancy remains unclear. Like $NaNbO_3$, the TO_2 mode in $KNbO_3$ is q independent along the [100] direction.[21] The zone-center TO_2 phonon energy is 24.8 meV for $KNbO_3$. First-principles calculations predicted that the TO_2 phonon energy is 14.3 meV in $NaNbO_3$.[14] The calculated TO_2 energy is 20% lower than the present experimental value. For $KNbO_3$ first-principles calculations reproduced the zone-center TO_2 phonon energy.[23,59,60] In the TO_2 mode, the K atom oscillates against all of the other atoms. The TO_2 mode in $NaNbO_3$ is expected to be dominated by the Na atom motion. In view of the A-site atomic mass, the difference in TO_2 energies suggests that the force constant between nearest-neighbor Na and oxygen atoms is weaker than that between K and oxygen atoms.

IV. CONCLUSION

We have investigated systematically the lattice dynamics of cubic $NaNbO_3$. The simultaneous softening of zone-boundary M_3 and R_{25} modes occurs in cubic $NaNbO_3$. These zone-boundary modes exhibit the gradual softening as the temperature is lowered $T_{c1}=913$ K. The inelastic diffuse scattering at the $M(0.5,0.5,0)$ point polarized along the $[1\bar{1}0]$ direction remains up to 9 meV, whereas the inelastic diffuse scattering at the M point polarized along the [001] direction is suppressed. Polarization dependence strongly suggests that the inelastic diffuse scattering at the M and R points is attributed to the dynamical motion of oxygen octahedra. The softening of zone-boundary modes corresponds to the X-ray diffuse scattering along the M-R line.[7,11] The elastic constants C_{ij} for $NaNbO_3$ are approximately equal to the corresponding values for $KNbO_3$. The $TO_1\Sigma_4$ phonon branch drops sharply near $\mathbf{q}=[0.15,0.15,0]$, and then merges into the TA Σ_4 phonon branch at $\mathbf{q}_c=[0.12,0.12,0]$. Two possible explanations for the steep drop are proposed. One is the precursor to the softening of zone-center TO_1 mode. Another explanation is the phonon instability associated with the T_1 to S phase transition at $T_{c3}=793$ K or the S to R phase transition at 753 K. The steep drop in the $TO_1\Sigma_4$ mode is basically similar to the waterfall phenomenon observed for Pb-based relaxors. The TA Δ_5 phonon in $NaNbO_3$ appears to overlap gradually with the $TO_1\Delta_5$ phonon with decreasing $\mathbf{q}$ in the $[\zeta,0,0]$ direction. The extreme broad LA and TA modes in $NaNbO_3$ contribute significantly to the inelastic diffuse scattering at Bragg points. The broadening of TA and TO modes are attributed to the anharmoicity of lattice vibrations. The coexistence of long-wavelength and zone-boundary phonon instabilities in the cubic phase is closely related to the complex sequence of phase transitions in $NaNbO_3$.

ACKNOWLEDGMENTS

We are grateful to N. Wakabayashi, H. Unoki, and D. Vanderbilt for stimulating discussions. We would like to thank Ryuichi Kato for his technical expertise in setting up the high-temperature furnace for neutron scattering experiments.

*tomeno@gipc.akita-u.ac.jp
†Present address: Graduate School of Science, Osaka University, Toyonaka, Osaka 560-0043, Japan.

[1] C. N. W. Darlington and K. S. Knight, Physica B **266**, 368 (1999).
[2] C. N. W. Darlington and K. S. Knight, Acta Crystallogr., Sect. B: Struct. Sci. **55**, 24 (1999).
[3] A. M. Glazer and H. D. Megaw, Acta Crystallogr., Sect. A: Cryst. Phys., Diffr., Theor. Gen. Crystallogr. **29**, 489 (1973).
[4] C. N. W. Darlington and H. D. Megaw, Acta Crystallogr., Sect. B: Struct. Crystallogr. Cryst. Chem. **29**, 2171 (1973).
[5] M. Ahtee, A. M. Glazer, and H. D. Megaw, Philos. Mag. **26**, 995 (1972).
[6] S. K. Mishra, N. Choudhury, S. L. Chaplot, P. S. R. Krishna, and R. Mittal, Phys. Rev. B **76**, 024110 (2007).
[7] F. Denoyer, R. Comès, and M. Lambert, Acta Crystallogr., Sect. A: Cryst. Phys., Diffr., Theor. Gen. Crystallogr. **27**, 414 (1971).
[8] A. M. Glazer and H. D. Megaw, Philos. Mag. **25**, 1119 (1972).
[9] A. M. Glazer, Acta Crystallogr., Sect. B: Struct. Crystallogr. Cryst. Chem. **28**, 3384 (1972).
[10] C. N. W. Darlington, Acta Crystallogr., Sect. A: Cryst. Phys., Diffr., Theor. Gen. Crystallogr. **58**, 66 (2002).
[11] K. Ishida and G. Honjo, J. Phys. Soc. Jpn. **34**, 1279 (1973).
[12] F. Denoyer, M. Lambert, R. Comes, and R. Currat, Solid State Commun. **18**, 441 (1976).
[13] F. Gervais, J. L. Servoin, J. F. Baumard, and F. Denoyer, Solid State Commun. **41**, 345 (1982).
[14] W. Zhong, R. D. King-Smith, and D. Vanderbilt, Phys. Rev. Lett. **72**, 3618 (1994).
[15] W. Zhong and D. Vanderbilt, Phys. Rev. Lett. **74**, 2587 (1995).
[16] D. Vanderbilt and W. Zhong, Ferroelectrics **206**, 181 (1998).
[17] A. C. Nunes, J. D. Axe, and G. Shirane, Ferroelectrics **2**, 291 (1971).
[18] M. D. Fontana, G. Dolling, G. E. Kugel, and C. Carabatos, Phys. Rev. B **20**, 3850 (1979).
[19] R. Currat, R. Comes, B. Dorner, and E. Wiesendanger, J. Phys. C **7**, 2521 (1974).
[20] R. Currat, H. Buhay, C. H. Perry, and A. M. Quittet, Phys. Rev. B **40**, 10741 (1989).
[21] M. Holma and H. Chen, J. Phys. Chem. Solids **57**, 1465 (1996).
[22] S. N. Gvasaliya, B. Roessli, R. A. Cowley, S. G. Lushnikov, A. Choubey, and P. Günter, JETP Lett. **80**, 355 (2004).
[23] R. Yu and H. Krakauer, Phys. Rev. Lett. **74**, 4067 (1995).
[24] A. Zheludev, RESLIB3.1, Oak Ridge National Laboratory.
[25] R. A. Cowley, Phys. Rev. **134**, A981 (1964).
[26] C. H. Perry, R. Currat, H. Buhay, R. M. Migoni, W. G. Stirling, and J. D. Axe, Phys. Rev. B **39**, 8666 (1989).
[27] G. Shirane and Y. Yamada, Phys. Rev. **177**, 858 (1969).
[28] P. Ghosez, E. Cockayne, U. V. Waghmare, and K. M. Rabe, Phys. Rev. B **60**, 836 (1999).
[29] I. Tomeno, Y. Ishii, Y. Tsunoda, and K. Oka, Phys. Rev. B **73**, 064116 (2006).
[30] R. D. Shannon, Acta Crystallogr., Sect. A: Cryst. Phys., Diffr., Theor. Gen. Crystallogr. **32**, 751 (1976).
[31] R. Comès and G. Shirane, Phys. Rev. B **5**, 1886 (1972).
[32] J. Harada, J. D. Axe, and G. Shirane, Phys. Rev. B **4**, 155 (1971).
[33] W. G. Stirling, J. Phys. C **5**, 2711 (1972).
[34] M. E. Hakiki, J. Eschbach, D. Rouxel, B. Vincent, S. Vialle, J. K. Kruger, O. Elmazria, and P. Alnot, Ferroelectrics **351**, 96 (2007).
[35] H. H. Barrett, Phys. Lett. **26A**, 217 (1968).
[36] Z. Li, S.-K. Chan, M. H. Grimsditch, and E. S. Zouboulis, J. Appl. Phys. **70**, 7327 (1991).
[37] R. O. Bell and G. Rupprecht, Phys. Rev. **129**, 90 (1963).
[38] Z. Li, M. Grimsditch, X. Xu, and S.-K. Chan, Ferroelectrics **141**, 313 (1993).
[39] O. Díeguez, K. M. Rabe, and D. Vanderbilt, Phys. Rev. B **72**, 144101 (2005).
[40] R. D. King-Smith and D. Vanderbilt, Phys. Rev. B **49**, 5828 (1994).
[41] S. Piskunov, E. Heifets, R. I. Elglits, and G. Borstel, Comput. Mater. Sci. **29**, 165 (2004).
[42] J. D. Axe, J. Harada, and G. Shirane, Phys. Rev. B **1**, 1227 (1970).
[43] I. Tomeno, S. Shimanuki, Y. Tsunoda, and Y. Ishii, J. Phys. Soc. Jpn. **70**, 1444 (2001).
[44] P. M. Gehring, S.-E. Park, and G. Shirane, Phys. Rev. B **63**, 224109 (2001).
[45] P. M. Gehring, S. Wakimoto, Z.-G. Ye, and G. Shirane, Phys. Rev. Lett. **87**, 277601 (2001).
[46] P. M. Gehring, S.-E. Park, and G. Shirane, Phys. Rev. Lett. **84**, 5216 (2000).
[47] J. Hlinka, S. Kamba, J. Petzelt, J. Kulda, C. A. Randall, and S. J. Zhang, Phys. Rev. Lett. **91**, 107602 (2003).
[48] T. Y. Koo, P. M. Gehring, G. Shirane, V. Kiryukhin, S.-G. Lee, and S.-W. Cheong, Phys. Rev. B **65**, 144113 (2002).
[49] C. Stock *et al.*, Phys. Rev. B **73**, 064107 (2006).
[50] R. Comès, M. Lambert, and A. Guinier, Solid State Commun. **6**, 715 (1968).
[51] R. Comès, M. Lambert, and A. Guinier, Acta Crystallogr., Sect. A: Cryst. Phys., Diffr., Theor. Gen. Crystallogr. **26**, 244 (1970).
[52] N. Takesue, M. Maglione, and H. Chen, Phys. Rev. B **51**, 6696 (1995).
[53] M. Holma, N. Takesue, and H. Chen, Ferroelectrics **164**, 237 (1995).
[54] S. Ravy, J.-P. Itié, A. Polian, and M. Hanfland, Phys. Rev. Lett. **99**, 117601 (2007).
[55] B. D. Chapman, E. A. Stern, S.-W. Han, J. O. Cross, G. T. Seidler, V. Gavrilyatchenko, R. V. Vedrinskii, and V. L. Kraizman, Phys. Rev. B **71**, 020102(R) (2005).
[56] V. A. Shuvaeva, Y. Azuma, K. Yagi, K. Sakaue, and H. Terauchi, J. Synchrotron Radiat. **8**, 833 (2001).
[57] V. A. Shuvaeva, K. Yanagi, K. Yagi, K. Sakaue, and H. Terauchi, J. Synchrotron Radiat. **6**, 367 (1999).
[58] V. A. Shuvaeva, K. Yanagi, K. Yagi, K. Sakaue, and H. Terauchi, Solid State Commun. **106**, 335 (1998).
[59] A. V. Postnikov, T. Neumann, and G. Borstel, Phys. Rev. B **50**, 758 (1994).
[60] C.-Z. Wang, R. Yu, and H. Krakauer, Phys. Rev. B **54**, 11161 (1996).